J. Comp. App. Res. Mech. Eng. Vol. 13. No. 2, pp. 191-206, 2024 *DOI: 10.22061/JCARME.2024.8784.2182*

SRTTU

Journal of Computational and Applied Research in Mechanical Engineering

jcarme.sru.ac.ir

JCARME

ISSN: 2228-7922

Research paper

Effect of concentric and eccentric porous layers on forced convection heat transfer and fluid flow around a solid cylinder

Alireza Alinezhad, Ataallah Soltani Goharrizi* and Ataallah Kamyabi

Department of Chemical Engineering, Faculty of Engineering, Shahid Bahonar University of Kerman, Kerman, 7618868366, Iran

Article info:

Article history:

Received: 25/01/2022

Accepted: 20/01/2024

Revised: 25/01/2024

Online: 27/01/2024

Keywords:

Porous media,

Darcy number,

Volume averaged equation,

Eccentricity,

Cross-flow.

***Corresponding author:**

a.soltani@uk.ac.ir

Abstract

In this paper, heat transfer and fluid flow around a solid cylinder wrapped with a porous layer in the channel were studied numerically by computational fluid dynamics. The homogeneous concentric and eccentric porous medium around a rigid and solid cylinder is supposed at local thermal equilibrium. The transport phenomena within the porous layer and volume-averaged equations were employed; however, the conservation laws of mass, momentum and energy were applied in the channel. The main purpose of this study is to analyze and compare the heat flux of concentric and eccentric porous layer in the Reynolds number range of 1 to 40 and Darcy numbers of 10^{-2} to 10^{-6}. It is found that with the decline of Darcy number, the vortex length is increased behind the solid cylinder surface. In addition, the heat flux rate of the cylinder is raised with the increase of Reynolds number. Finally, the results showed that the average Nusselt numbers in different Darcy and Reynolds numbers are higher in the eccentric porous layer than in the concentric porous layer. For example, our findings show that in $Da = 10^{-5}$, $Re = 40$ and $d = 0{,}07\ m$, the average Nusselt number in the eccentric porous layer is 7.5% higher than the concentric porous layer.

1. Introduction

In the past years, a variety of numerical and experimental studies on convective heat transfer and fluid flow in porous-coated channels and cylinder surfaces have been done for concentric and eccentric forms. The behavior of fluid flow in the porous medium is very remarkable because of its unique structure and applications in various fields such as the design of heat exchangers, energy storage units, fuel cells, thermal management in the cooling of electronic equipment, and improvement of the performance of heat transfer systems. For this reason, numerical and experimental studies have been carried out on this phenomenon [1-8] .

Many studies have been published about the fluid flow and heat transfer rate in various porous media by several researchers. For example, Bhattacharyya *et al.* [1] numerically studied fluid flow inside and over a porous layer around a solid cylinder surface within the Reynolds number range of 1-40 and the porosities of 0.629-0.999. They found that by declining

porosity and increasing Reynolds number, the separation point (the separation angle) on the porous layer around the solid cylinder surface could decrease. Bhattacharyya and Singh [2] also numerically offered heat transfer from a porous layer with high conductivity coefficient and considered porosity around a solid cylinder. The optimal amount of porous layer thickness to improve the heat transfer rate was obtained. Their results indicated that a high porosity layer with high conductivity coefficient ($R_c = k_{eff} / k_f \geq 5$) could increase the heat transfer rate, even at low permeability (Da = 10^{-5}). They also found that by increasing the Reynolds number, the formation of periodic vortex could be formed.

Similarly Rashidi *et al.* [3] conducted a numerical study of fluid flow and heat transfer around a cylinder covered with a porous layer. They found that the thermal performance of heat exchangers with high permeability and thermal conductivity of the porous layer was improved. Valipour and Zare Ghadi [9] also numerically simulated the forced convective heat transfer around and through the porous cylinder in the Reynolds number range of 1 to 40 and $10^{-6} \leq Da \leq 10^{-2}$. Their numerical results showed that with the rise of Darcy number, the local and average Nusselt numbers increased.

Rong *et al.* [10] performed a numerical study on a square cylinder covered by a porous layer. They showed that by increasing the porous layer thickness in $Da \geq 10^{-4}$, the amount of drag and lift coefficient increased and the flow fluid could penetrate into the porous layer easily. Alvandifar *et al.* [11] numerically investigated a tube bank with 5 rows of tubes wrapped by metal foam layers inside air-cooled heat exchangers. Their results showed that heat transfer in the tubes covered with a thin metal foam layer was much arger than in bare tube banks.

Another numerical investigation was done by Odabaee *et al.* [12] for the heat transfer rate from a single metal-foam-wrapped solid cylinder in crossflow. Their results showed that the heat transfer rate increased, as a reasult they realized that pressure drop increased by raising the porous layer thickness. Rahmati *et al.* [13] also numerically studied heat transfer rates from a solid cylinder covered with metal foam. They assumed the local thermal equilibrium between the fluid flow and porous layer surface in the cross-flow of the turbulent regime. Their results showed that the Nusselt number of the solid cylinder with a metal porous layer was almost 10 times larger than the bar tube without wrapping a metal porous layer.

Ait Saada *et al.* [14] investigated the effects of natural convection on heat losses and its improvement in a horizontal cylinder with fibrous or porous coating. In their reaserch, the flow movement and heat transfer coefficient were analyzed. According to their numerical results, when the permeability of a limited porous coating has an equivalent to a Darcy number greater than 10^{-6}, the conduction and convection theory combined with the non-Darcian model should be applied.

Al-Sumaily *et al.* [15] carried out a numerical study to investigate the forced convection heat transfer from a packed bed of spherical particles accommodated in a circular cylinder. They concluded that using a porous medium with large particle diameters increased heat transfer and decreased the pressure drop. Pedras and Lemos [16] developed turbulent models for fluid flow in a porous medium in two various ways. The first one was using the macroscopic equations employing the extended Darcy-Forchheimer model and the second one was Reynolds-averaged equations.

Chen *et al.* [17] investigated heat transfer of fluctuating tube bundles wrapped with metallic foam, experimentally. According to this experimental study, they concluded that the Nusselt number was raised gradually with increasing the amount of fluid flow permeability because of high porosity in the porous layer. In another experimental study, Al-Salem *et al.* [18] investigated the effect of porosity and thickness of an aluminum porous layer to improve heat transfer performance of a heated horizontal cylinder with constant heat flux. In this experimental research, they concluded that the average Nusselt number increased with raising the porosity of the aluminum layer and also with the addition of the porous layer, the amount of pressure loss decreased.

Calmidi and Mahajan [19] as well as Zhao *et al.* [20] carried out numerical and experimental analyses on the forced convection in high porosity metal foams. The thermal spread was affected by increasing heat transfer. In addition, this study showed that pore density and various materials could affect the heat transfer and pressure drop. Recently, Ebrahimi *et al.* [21] analyzed heat transfer characteristics of elastically-mounted solid cylinders covered with concentric porous layers numerically. In their

research, the range of various diameters (d=0.20, 0.5, 1) and the Darcy number ($10^{-6} \leq Da \leq 10^{-2}$) were considered, respectively. Their simulation showed that by increasing the porous layer diameter of the solid cylinder displacement domain, the amount of average Nusselt number declined. Keshtkar and Dadkhodazadeh [22] investigated the effects of porous gas heat exchangers on fluid flow and heat transfer for two symmetric and asymmetric with the regulation of barriers in the cross-flow state by lattice Boltzmann method (LBM). In their study, the results show that with increases in Darcy number, permeability within porous gas heat exchanger (PGHE) and natural convective heat transfer rate were raised, respectively. Also, analyzing the arrangement of barriers indicated that the convective heat transfer rate in the asymmetric arrangement was better than in the symmetric arrangement.

The review of various articles shows that most of them have considered heat transfer and fluid flow around a cylinder covered by a concentric porous layer. The main purpose of this research was to investigate the effects of eccentric porous layers with different diameters on heat transfer rate and laminar fluid flow. To achieve the objectives of this study, parameters such as the permeability of the eccentric porous layer thickness, the length of recirculation region, tangential and radial velocity, temperature distribution on the surface of the rigid and porous layer, heat transfer flux, and the average Nusselt number in the range of different Darcy and Reynolds numbers have been investigated.

2. Problem definition

2.1. Physical model

The geometry of problem consists of a long, rigid, and solid cylinder covered with a concentric and eccentric porous layer in the channel as shown in Fig. 1, respectively. In this current research, the problem was modeled as two-dimensional (2-D). To decrease the effects of channel walls on the flow near the solid cylinder, the ratio of channel height (W) to the diameter (D) of the solid cylinder must be high ($\frac{W}{D} = \frac{0,5}{0,05} = 10$) [23], therefore, we ignored it in this study. We considered the constant temperature of the solid cylinder surface at 313K and the temperature of inlet fluid flow was fixed at 293K. Also, the diameter of the solid cylinder is 0.05 m and the characteristic of the channel is 0.5×1 m. The boundary conditions included no-slip at the adjacent surface of the channel (upper and lower surface) and the solid cylinder surface. A laminar flow was considered to run around the isothermal cylinder. The porous zone around the cylinder was assumed to be homogeneous and isotropic. All fluid properties were considered to be constant. The temperature of solid phase was equal to the fluid phase (local thermal equilibrium (LTE)).

2.2. Governing equations

Equations governing the clear fluid zones are Navier-Stokes equations and those that govern the porous medium zones are the volume averaged equations.

The clear fluid and porous medium domains are indicated by the subscripts (1) and (2), respectively. The mass conservation equation in region 1 (clear fluid) [3]:

$$\frac{\partial}{\partial r}(ru_1) + \frac{\partial}{\partial \theta}(v_1) = 0 \quad (1)$$

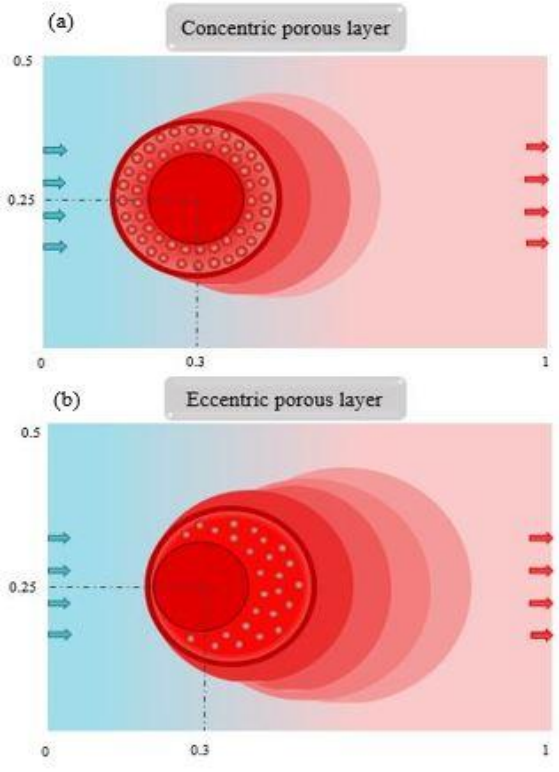

Fig. 1. Schematic of the solid cylindrical geometry; (a) concentric porous layer and (b) eccentric porous layer.

And the momentum equations in the r and θ direction [3]:

$$\left(\frac{v_1}{r}\frac{\partial u_1}{\partial \theta}+u_1\frac{\partial u_1}{\partial r}-\frac{v_1^2}{r}\right)=-\frac{\partial p_1}{\partial r}+\frac{2}{Re}\left(\frac{\partial^2 u_1}{\partial r^2}+\frac{1}{r}\frac{\partial u_1}{\partial r}+\frac{1}{r^2}\frac{\partial^2 u_1}{\partial \theta^2}-\frac{2}{r^2}\frac{\partial v_1}{\partial \theta}-\frac{u_1}{r^2}\right) \quad (2)$$

$$\left(\frac{v_1}{r}\frac{\partial v_1}{\partial \theta}+u_1\frac{\partial v_1}{\partial r}+\frac{u_1 v_1}{r}\right)=-\frac{1}{r}\frac{\partial p_1}{\partial \theta}+\frac{2}{Re}\left(\frac{\partial^2 v_1}{\partial r^2}+\frac{1}{r}\frac{\partial v_1}{\partial r}+\frac{1}{r^2}\frac{\partial^2 v_1}{\partial \theta^2}+\frac{2}{r^2}\frac{\partial u_1}{\partial \theta}-\frac{v_1}{r^2}\right) \quad (3)$$

The energy equation in region 1 can be written as [3]:

$$\left(u_1\frac{\partial T_1}{\partial r}+\frac{v_1}{r}\frac{\partial T_1}{\partial \theta}\right)=\frac{2}{RePr}\left(\frac{\partial^2 T_1}{\partial r^2}+\frac{1}{r}\frac{\partial T_1}{\partial r}+\frac{1}{r^2}\frac{\partial^2 T_1}{\partial \theta^2}\right) \quad (4)$$

In region 2 (the porous medium region), the volume-averaged mass conservation equation becomes [3]:

$$\frac{\partial}{\partial r}(ru_2)+\frac{\partial}{\partial \theta}(v_1)=0 \quad (5)$$

$$\frac{1}{\varepsilon}\left(\frac{v_2}{r}\frac{\partial u_2}{\partial \theta}+u_2\frac{\partial u_2}{\partial r}-\frac{v_2^2}{r}\right)=-\varepsilon\frac{\partial p_2}{\partial r}+\Lambda\frac{2\varepsilon}{Re}\left(\frac{\partial^2 u_2}{\partial r^2}+\frac{1}{r}\frac{\partial u_2}{\partial r}+\frac{1}{r^2}\frac{\partial^2 u_2}{\partial \theta^2}-\frac{2}{r^2}\frac{\partial v_2}{\partial \theta}-\frac{u_2}{r^2}\right)-\frac{\varepsilon}{2ReDa}u_2-\frac{\varepsilon C_F}{2\sqrt{Da}}\sqrt{u_2^2+v_2^2}\,u_2 \quad (6)$$

$$\frac{1}{\varepsilon}\left(\frac{v_2}{r}\frac{\partial v_2}{\partial \theta}+u_2\frac{\partial v_2}{\partial r}+\frac{u_2 v_2}{r}\right)=-\frac{\varepsilon}{r}\frac{\partial p_2}{\partial \theta}+\Lambda\frac{2\varepsilon}{Re}\left(\frac{\partial^2 v_2}{\partial r^2}+\frac{1}{r}\frac{\partial v_2}{\partial r}+\frac{1}{r^2}\frac{\partial^2 v_2}{\partial \theta^2}+\frac{2}{r^2}\frac{\partial u_2}{\partial \theta}-\frac{v_2}{r^2}\right)-\frac{\varepsilon}{2ReDa}v_2-\frac{\varepsilon C_F}{2\sqrt{Da}}\sqrt{u_2^2+v_2^2}\,v_2 \quad (7)$$

The energy equation with the local thermal equilibrium assumption [3]:

$$\left(u_2\frac{\partial T_2}{\partial r}+\frac{v_2}{r}\frac{\partial T_2}{\partial \theta}\right)=\frac{2R_c}{RePr}\left(\frac{\partial^2 T_2}{\partial r^2}+\frac{1}{r}\frac{\partial T_2}{\partial r}+\frac{1}{r^2}\frac{\partial^2 T_2}{\partial \theta^2}\right) \quad (8)$$

The volume-averaged fluid velocity, $\vec{V}$ inside the porous region with the porosity (φ = ε) is related to the fluid velocity ($\vec{v}$), through the Dupuit-Forchheimer relationship, as $\vec{v}=\varphi\vec{V}$. Here we used the Ergun correlation to calculate the Forchheimer coefficient, C_F [24]:

$$C_F=\frac{1{,}75}{\sqrt{150\varphi^3}} \quad (9)$$

The permeability of the porous medium is calculated from the Kozeny–Carmen relation, as shown below [25]:

$$K=\frac{d_p^2\varphi^3}{150(1-\varphi)^2} \quad (10)$$

where K is the permeability and d_p is the average particle size in the porous layer.

2.3. Boundary conditions

Dimensions of the computational domain should be selected in a way to minimize the effects of the outer boundaries. The size of the channel to the two-dimensional computational domain is 0.5m × 1m. The governing equations (1) – (8) are subjected to the following boundary conditions.

The hydrodynamic and thermal boundary conditions of the inlet fluid flow at the entrance of the channel:

$$u=U_\infty \qquad v=0 \qquad T=T_\infty \quad (11)$$

The fluid flow is both hydraulically and thermally fully-developed in the r direction. The hydrodynamic and thermal boundary conditions at the upper and lower boundaries are symmetric:

$$\frac{\partial u_1}{\partial r}=0 \qquad \frac{\partial v_1}{\partial r}=0 \qquad T_1=T_\infty \quad (12)$$

no-slip wall boundary condition with a fixed wall temperature on the solid cylinder surface:

$$u_2=0 \qquad v_2=0 \qquad T_2=T_w \quad (13)$$

along the upstream boundary (uniform flow):

$$0<\theta<\frac{\pi}{4}\Rightarrow u_1=-\cos\theta \quad v_1=\sin\theta \quad T_1=T_\infty \quad (14)$$

2.4. Coupling conditions

In the current study, we assumed the continuity of velocity, shear stress, temperature and heat

flux here at the interface between the porous layer and the fluid area:

$$u_1 = u_2 \quad v_1 = v_2 \tag{15}$$

$$\mu_f \frac{\partial v_1}{\partial r} = \frac{\mu_f}{\varphi} \frac{\partial v_2}{\partial r} \tag{16}$$

$$T_1 = T_2 \tag{17}$$

$$\frac{\partial T_1}{\partial r} = \frac{\varphi k_f + (1-\varphi) k_s}{k_f} \frac{\partial T_2}{\partial r} \quad \frac{\partial T_1}{\partial \theta} = \frac{\varphi k_f + (1-\varphi) k_s}{k_f} \frac{\partial T_2}{\partial \theta} \tag{18}$$

2.5. Numerical method

In this paper, numerical investigations were obtained by using the finite volume method-based solver. The steady, pressure-based solver was chosen to solve the thermo-fluid-dynamic problem discussed in this study. In the porous zone, to solve the fluid flow, the energy equations, Darcy-Brinkmann-Forchheimer model, and local thermal equilibrium (LTE) were used and activated. SIMPLE algorithm was used to couple the pressure and the velocity terms for the pressure correction equation. The least squares cell-based method was applied to construct the values of a scalar at the cell faces. A second-order discretization scheme for pressure and a second-order upwind discretization scheme for momentum and energy were considered.

2.6. Grid independent study

To ensure that the simulation results are independent of the mesh size, the values of the heat flux on the solid cylinder surface wrapped with a eccentric porous layer were calculated; so, we found that the independence of the mesh size was reasonable. Then, we chose the number of cells (76360) to avoid the waste of time and cost in this research. Also, we made a comparison of heat flux for different grids according to the Reynolds and porosity of 40 and 0.70 as shown in Table 1, respectively.

2.7. Validation

In the first stage of validation, the numerical data have been compared with the experimental data that the Nusselt number distribution passes through a solid cylinder without a porous layer. Fig. 2 shows the investigations of other studies where the numerical and experimental data for Nusselt number distribution are considered. Then, in the present study, three various diameters of the rigid layers covered around the solid cylinder in both concentric and eccentric states were considered and compared with the numerical data [23]. Table 2 shows the variable diameter of the layers with the amounts of heat flux in both concentric and eccentric states. The amount of deviation in Table 2 is obtained according to Eq. (19).

$$\text{Deviation (\%)} = \frac{Data\ (\text{Simulation}) - Data\ (\text{present work})}{Data\ (\text{Simulation})} \times 100 \tag{19}$$

In the final stage of validation, the results of the tangential and radial velocity distribution on the surface of concentric porous layer covered around the solid cylinder with Darcy number of 10^{-2} had been compared with the numerical results [3]. The results of this comparison for tangential and radial velocities show in Figs. 3, 4, respectively.

Table 1. Comparison of heat flux on the cylinder surface for different grids.

Deviation (%)	Heat flux ($\frac{w}{m^2}$)	Number of cells
23.14	76360	0.08
23.12	108170	
23.04	326875	0.08
23.06	340900	

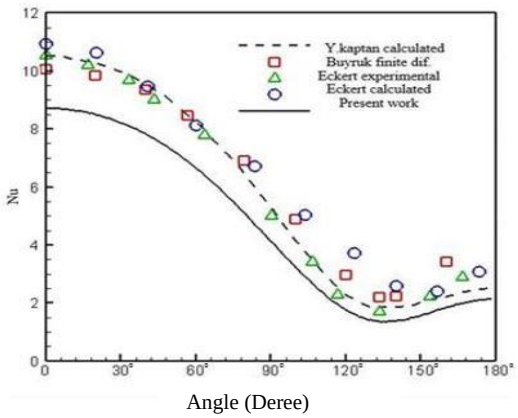

Fig. 2. Distribution of nusselt number on the clean tube parameter for other experimental and numerical studies [23] and the present work.

Table 2. Numerical validation of the heat flux transfer results.

Type of symmetry	Diameter (m)	Heat transfer flux on the surface of the rigid layer ($\frac{w}{m^2}$)		Deviation (%)
		Simulation [23]	Simulation (present work)	
Concentric	0.07	32.13	30.60	4.7
Eccentric	0.07	32.25	31.58	2.07
Concentric	0.08	26.36	25.19	4.4
Eccentric	0.08	27.15	25.90	4.6
Concentric	0.09	22.14	21.30	4.2
Eccentric	0.09	22.82	21.82	4.3

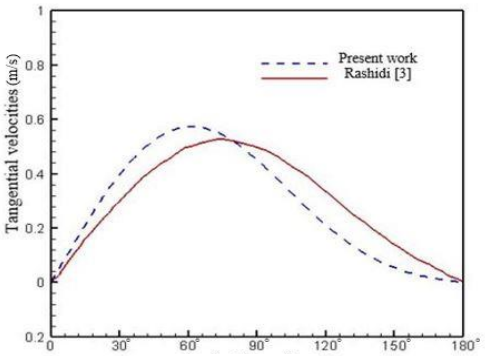

Fig. 3. The comparison of tangential velocity distribution on the porous layer with numerical results.

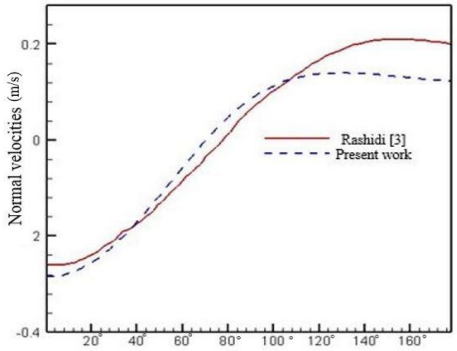

Fig. 4. The comparison of radial velocity distribution on the porous layer with numerical results.

3. Results and discussion

3.1. Hydrodynamic results

Fig. 5 shows the streamlines of fluid flow with Re=1 and Re=40 passing through the eccentric porous layer and the solid cylinder. In this case, the streamlines go curved surrounding the solid cylinder surface and the porous layer. In fact, it could be said that the fluid flow was entirely wrapped around the solid cylinder along with the porous layer.

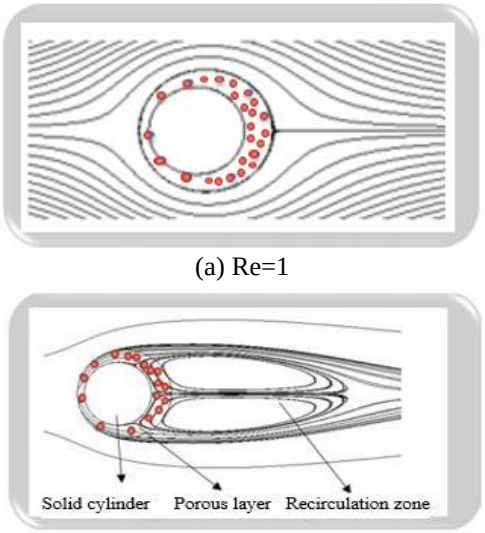

(a) Re=1

(b) Re=40

Fig. 5. Schematic of the vortexes formed behind the solid cylinder in (a) *Re*=1 and (b) *Re*=40.

However, if the Reynolds number increased, the separation of the boundary layer would take place. Also, the formation of the wake behind the solid cylinder was created

In Fig. 6 the effects of the Reynolds number on the streamlines and the length of the vortexes behind the solid cylinder and the outer surface of the eccentric porous layer for all four distinct states (a) $Da=10^{-2}$ (b) $Da=10^{-3}$ (c) $Da=10^{-5}$ (d) $Da=10^{-6}$ with the same diameter of the porous layer (d=0.07m) are shown. According to the Darcy number, it could be seen that with the increase of the Darcy number, the amount of the fluid penetration in the porous layer raised and the fluid flow could transform freely within the porous layer. As shown in Fig. 6, at low Reynolds number (Re=1), the streamlines in each of the four states (a, b, c, d at Re = 1) had stuck to the outer porous layer surface, and no vortex was created behind the solid cylinder.

(a)

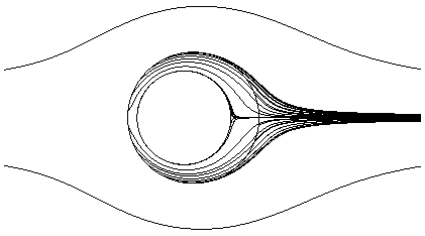

$Da=10^{-2}$ $Re=1$

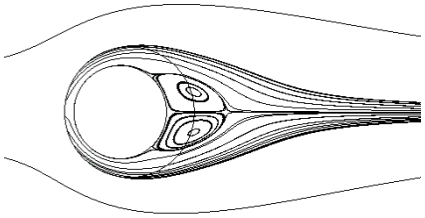

$Da=10^{-2}$ $Re=10$

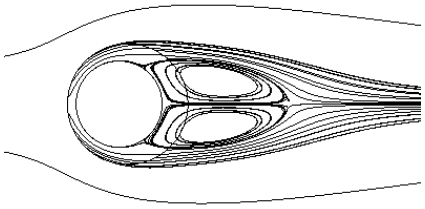

$Da=10^{-2}$ $Re=20$

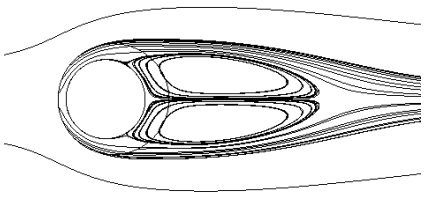

$Da=10^{-2}$ $Re=30$

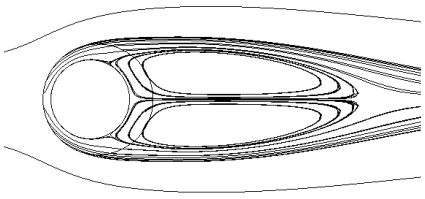

$Da=10^{-2}$ $Re=40$

(b)

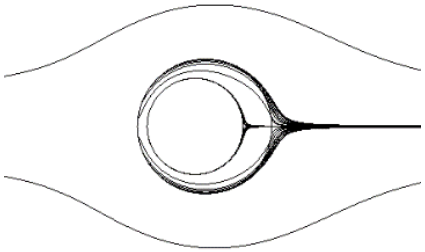

$Da=10^{-3}$ $Re=1$

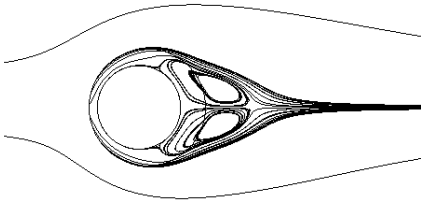

$Da=10^{-3}$ $Re=10$

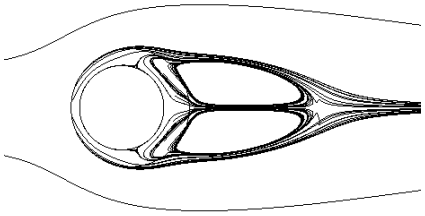

$Da=10^{-3}$ $Re=20$

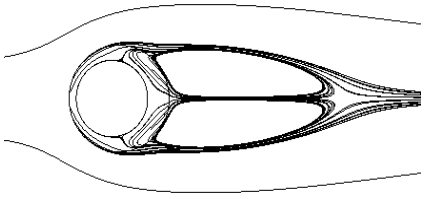

$Da=10^{-3}$ $Re=30$

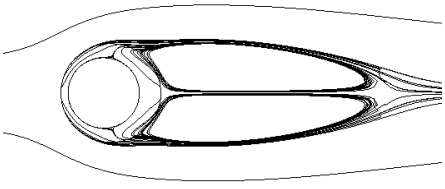

$Da=10^{-3}$ $Re=40$

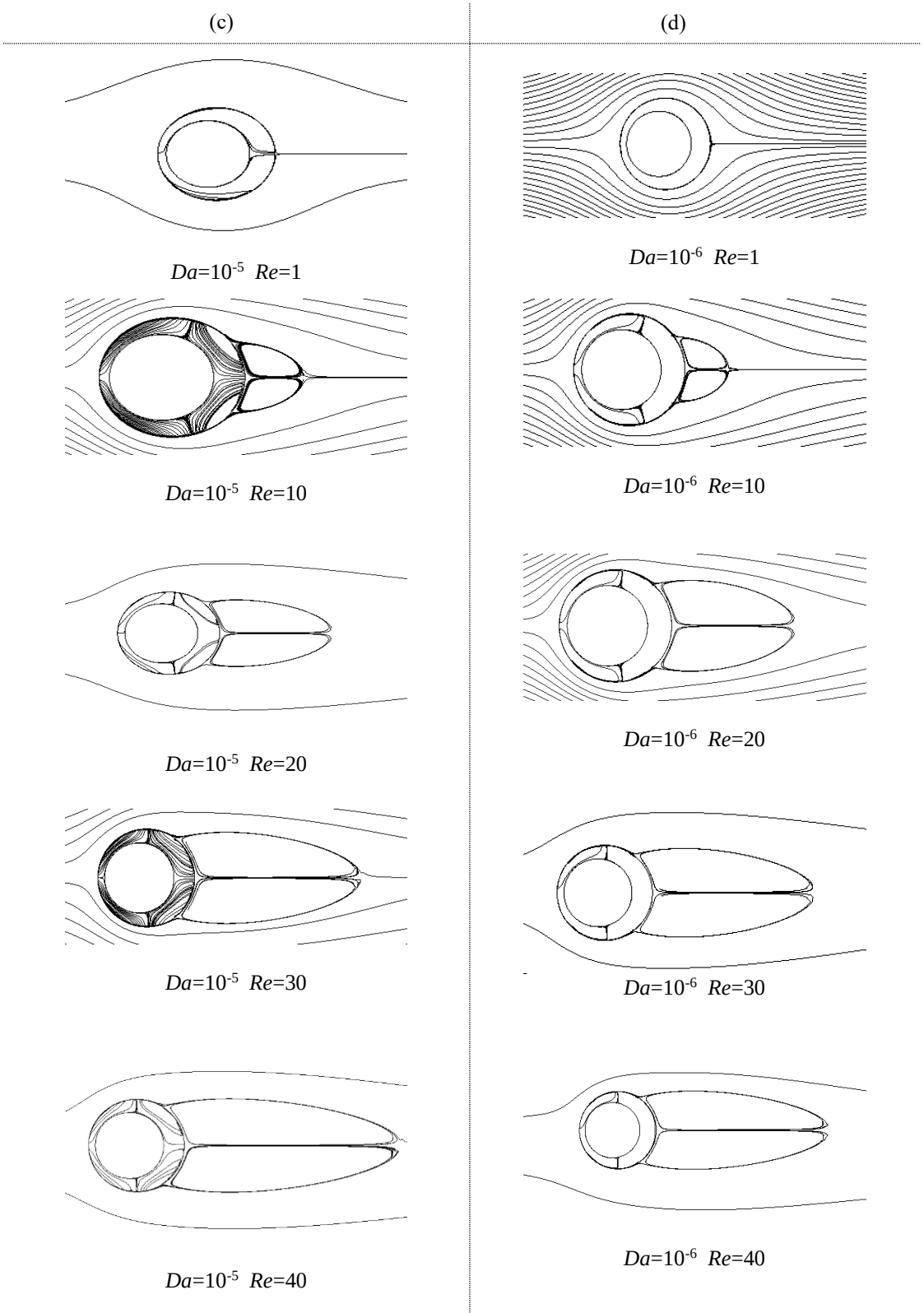

Fig. 6. Configuration of streamlines in various Reynolds (*Re*=1, 10, 20, 30, 40) for (a) $Da=10^{-2}$, (b) $Da=10^{-3}$, (c) $Da=10^{-5}$, and (d) $Da=10^{-6}$

As the Reynolds number was increased (Re = 10, 20, 30 and 40), a pair of vortexes was formed behind the solid cylinder and the porous layer. So it could be seen that by raising the Darcy number, the quantity of fluid penetration in the porous layer was expanded. Similarly, by raising the Reynolds number, the vortex length was developed behind the solid cylinder and the porous layer. Although it could be concluded that with the decrease in the Darcy number, the vortex length increases, meaning that a pair of vortexes stretches from the porous layer into the fluid field with the greater Darcy number. Also, the vortexes would be closer to the solid cylinder surface.

Figs. 7 and 8 show the effects of Darcy number on the distribution of tangential and radial velocities on the eccentric porous layer surface. As Darcy number gradually increased, the measure of vertical velocities on the eccentric porous layer surface raised, On the other hand, it also seemed that the distribution of tangential velocities in $Da=10^{-2}$ and $Da=10^{-3}$ in the direction of their velocity around an angle of 80° became in reverse. From both Figs. 7 and 8, it can also be concluded the porous layer surface and the rigid layer surface were identically at lower Darcy numbers because the permeability on the eccentric porous layer surface was decreased. At the result, on the eccentric porous layer surface created the semi-slip boundary condition and the simulated data of the tangential and normal velocities became approximately zero.

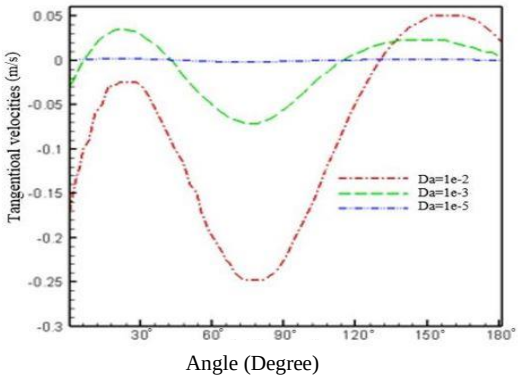

Fig. 7. Tangential velocities on the eccentric porous layer surface with a diameter of 0.09m and Re= 40.

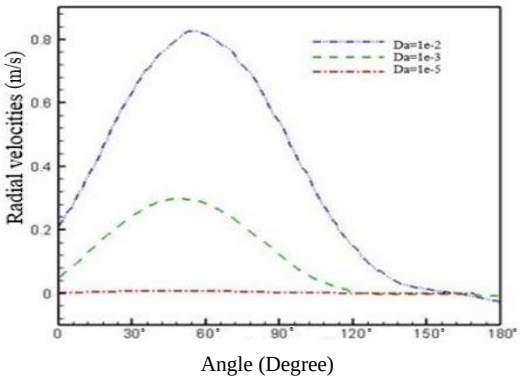

Fig. 8. Radial velocities on the eccentric porous layer surface with a diameter of 0.09m and Re= 40.

3.2. Heat transfer results

3.2.1. Temperature distribution

A comparison of temperature distribution on the eccentric porous layer with the eccentric rigid layer was conducted and shown in Fig. 9(a) and (b), respectively. The variation in the Reynolds number could change the profile of temperature distribution and temperature contour lines. The results are shown in Fig. 9(a) and (b). Fig. 9(a) shows the temperature distribution around the solid cylinder covered by an eccentric porous layer with Da = 10^{-2}. Fig. 9(a) shows the temperature distribution around the solid cylinder covered by an eccentric porous layer with $Da=10^{-2}$.

Fig. 9(b) displays temperature distribution around the solid cylinder wrapped with an eccentric rigid layer. In both cases, the temperature distribution in distinct Reynolds numbers ($1 \leq R_e \leq 40$) and the same diameter was analyzed. We can see that the temperature distribution of the inner and outer rigid layer surface was much more than the inner and outer of the porous layer surface. In fact, if the layer surrounding the solid cylinder is considered rigid, the greater volume of the fluid flow passing through the layer surface can be under the influence of the cylinder temperature.

Fig. 10 shows temperature distribution on the different rigid layer diameters and porous layer diameters with the same Reynolds number (Re=20). It could be concluded that the temperature distribution on the rigid layer surface was higher than the temperature distribution on the porous layer surface, meaning that the conduction of heat transfer in the rigid state was much more than the porous state.

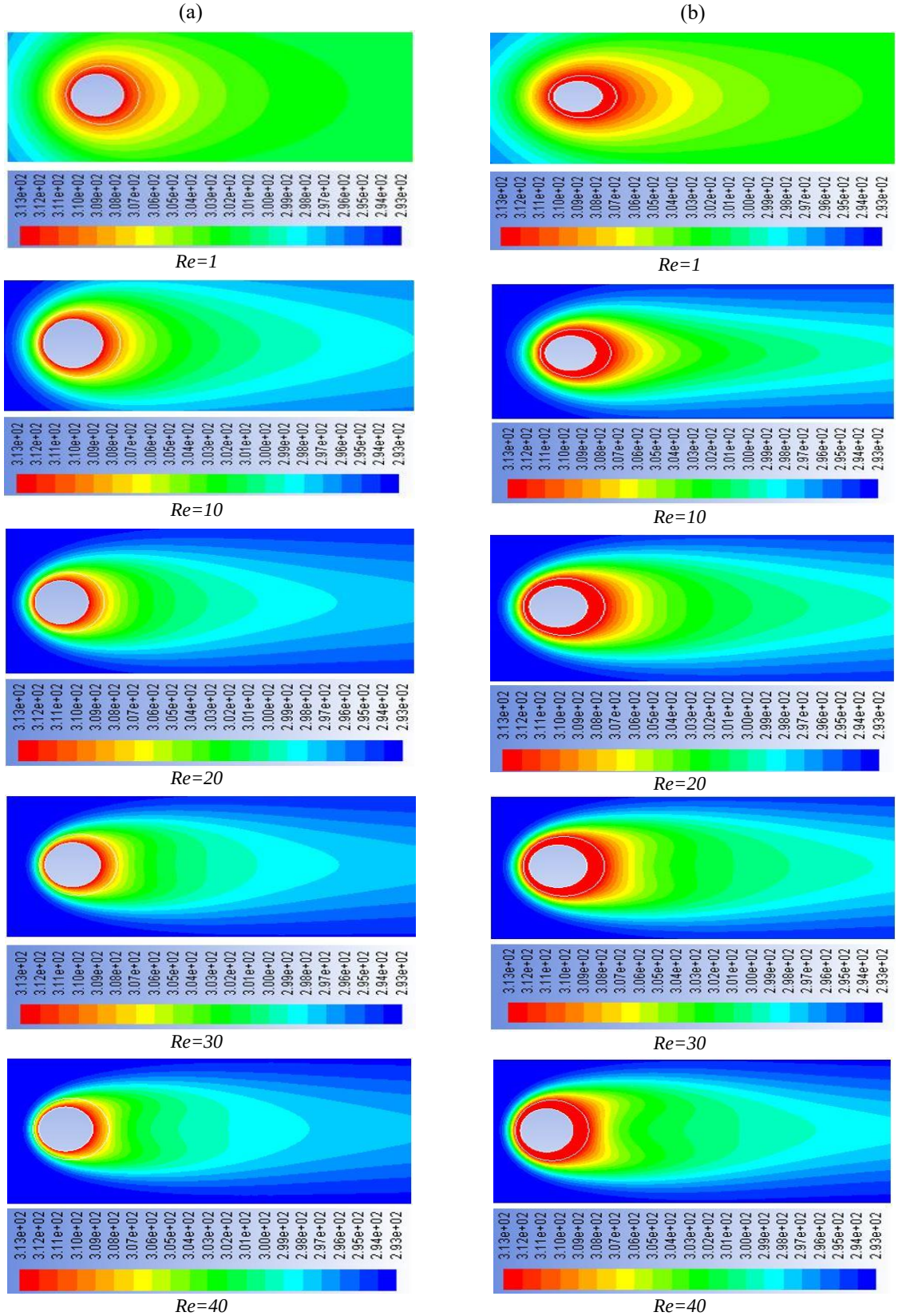

Fig. 9. The temperature distribution for an eccentric (a) porous layer and (b) rigid layer; diameter: 0.07 m and $Da=10^{-2}$.

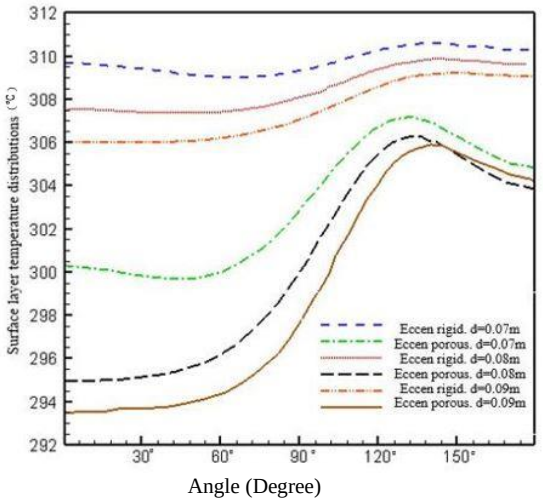

Fig. 10. Distribution of temperature on the surface of rigid and porous layers at Da=10^{-2}.

3.2.2. Heat transfer flux

The effects of Darcy and Reynolds numbers on the heat transfer flux from the cylinder surface to the diameters of concentric and eccentric porous layer states were accomplished by the simulated methods. Tables 3 and 4 show the heat transfer flux from the solid cylinder surface in the various Darcy numbers and Reynolds numbers with different diameters, respectively. The results were obtained by the simulated methods in Tables 3 and 4 which are as follows:

1. In the solid cylinder with constant wall temperature, by raising the Darcy number, the heat transfer flux through the cylinder could be increased.
2. In the constant Darcy number, with the increase in the diameter of the porous layer, the heat transfer flux passing through the cylinder was dropped.
3. By increasing the Reynolds number of the porous layer in a constant diameter, the heat transfer flux of the solid cylinder was raised, too.
4. In the constant Reynolds number, with the increase in the diameter of the porous layer, the heat transfer flux of the solid cylinder was decreased.
5. The main result was that the amount of the heat transfer flux of the solid cylinder into the fluid field in the eccentric porous layer state was five percent (5%) higher than that concentric porous layer state.

Rashidi *et al.* [3] reported the heat transfer flux distribution in the concentric porous layer, in this work we obtained the heat transfer flux distribution in the eccentric porous layer, which increased the heat transfer flux in the same diameters, same Reynolds number, and same Darcy number compared to the work of Rashidi *et al.* [3].

The distribution of the heat transfer flux on the solid cylinder surface in the two types of concentric and eccentric porous layers was analyzed. Fig. 11 shows the heat flux distribution on the solid cylinder surface covered by a concentric and eccentric porous layer with the Reynolds number and Darcy number considered 40 and 10^{-2}, respectively. The average heat transfer flux from the concentric porous layer state was obtained at 35.29 w/m^2 (d=0.07m), 31.03 w/m^2 (d=0.08m), and 28.79 w/m^2 (d=0.09m). Also, for the eccentric porous layer state, the average heat transfer flux was achieved at 39.52 w/m^2 (d=0.07m), 36.69 w/m^2 (d=0.08m), and 34.92 w/m^2 (d=0.09m). According to the simulated results, with the increase in the porous layer diameter, the overall convection heat transfer rate declined as well and with increasing the angle of direction fluid flow along the cylinder it decreased gradually.

The heat transfer flux distribution on the solid cylinder surface with different Reynolds numbers is shown in Fig. 12.

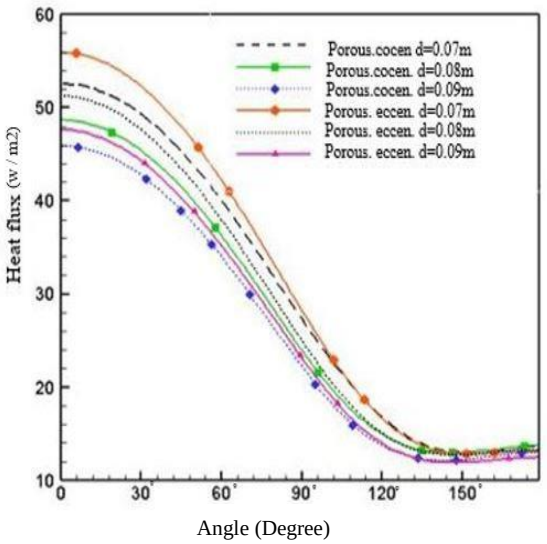

Fig. 11. Heat transfer flux from the solid cylinder surface.

Table 3. Simulated results for the heat transfer flux (w/m^2) in Re = 40.

Type of symmetry	Dameter (m)	$Da=10^{-2}$	$Da=10^{-3}$	$Da=10^{-4}$	$Da=10^{-5}$	$Da=10^{-6}$
Concentric	0.07	29.94	25.25	24.06	23.85	23.82
Concentric	0.08	27.41	22.24	21.27	21.12	21.10
Concentric	0.09	25.74	20.15	19.30	19.20	19.18
Eccentric	0.07	31.14	27.14	25.77	25.49	25.45
Eccentric	0.08	28.45	23.49	22.40	22.23	22.21
Eccentric	0.09	26.45	21.02	20.08	19.96	19.95

Table 4 . Simulated results for the heat transfer flux (w/m^2) in Da = 10^{-2}.

Type of symmetry	Diameter (m)	*Re*=1	*Re*=10	*Re*=20	*Re*=30	*Re*=40
Concentric	0.07	9.22	17.64	23.42	26.91	29.94
Concentric	0.08	9.09	17.48	21.43	24.56	27.46
Concentric	0.09	8.96	16.40	19.88	22.85	25.74
Eccentric	0.07	9.23	19.11	24.17	27.93	31.14
Eccentric	0.08	9.10	17.87	22.16	25.48	28.45
Eccentric	0.09	8.97	16.75	20.48	23.55	26.45

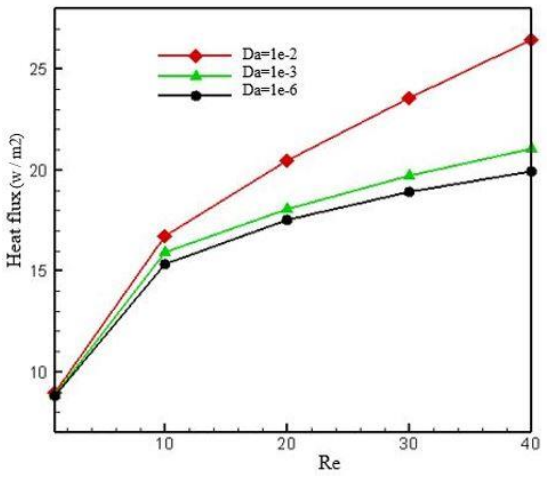

Fig. 12. Heat transfer flux on the solid cylinder surface with different Darcy and Reynolds numbers.

3.2.3. Nusselt number

The solid cylinder surface was maintained at a fixed temperature. The average heat flux of the cylinder surface to the fluid phase is shown in terms of various Reynolds numbers and Darcy numbers. According to the current numerical study, for an eccentric porous layer with a constant diameter (d = 0.09 m), it can be concluded that by increasing the Reynolds number, the heat flux of the cylinder increases. Also, the average heat transfer flux surface ratio in Da=10^{-2} is greater than Da=10^{-3} and Da=10^{-6}. Fig. 13 shows the simulated results for the average Nusselt number with the variation of Darcy number in the various concentric and eccentric porous layer diameters.With the increase of the Darcy number, the average Nusselt number was raised. Similarly, as the porosity of the porous layer increased, fluid penetration and forced convection heat transfer were developed. Also, we found that for greater Darcy numbers the average Nusselt number was increased faster. On the other hand, the effects of Darcy numbers higher than 10^{-4} was considerable in comparison to the average Nusselt number lower than 10^{-4}.

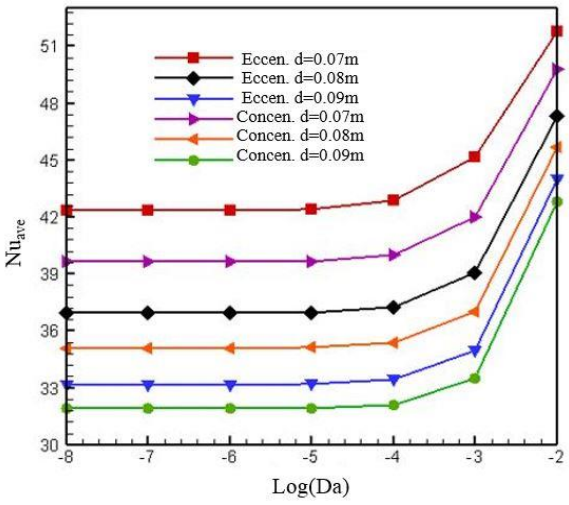

Fig. 13. The distribution of the average Nusselt number on the solid cylinder surface with the various diameters of eccentric and concentric porous layer Re=40.

Another remarkable point in Fig. 13 is that in a constant diameter and a fixed Darcy number, the effects of the eccentric porous layer on the Nusselt number would be greater than the one on the concentric porous layer. In the lower Darcy numbers, the porous layer behaves like that of a solid rigid layer because in the lower Darcy numbers, penetration declined.

According to Fig. 14, regarding different values of the Reynolds number for the porous layer, the numerical simulation of the Nusselt number is shown in relation to the Darcy number. It can be seen in Fig. 14 that with increasing the Darcy number associated with the eccentric porous layer with a diameter of 0.09, the average Nusselt number raised for all values related to the Reynolds parameters. As shown in Fig. 14, the average Nusselt number for $Da \geq 10^{-4}$ was increased with a steeper slope. Also, the effects of the Reynolds number on increasing the Nusselt number was more significant for $Da \geq 10^{-4}$. In a fixed Darcy number, with the increase of the Reynolds number, the overall heat transfer rate from the surface to the fluid was greater.

Fig. 15 shows the changes of the average Nusselt number relative to the Reynolds number changes for different values of the diameter of the porous layer in the concentric and eccentric states in constant Darcy number ($Da= 10^{-2}$). We found that with increasing the Reynolds number, the means of all different values of the concentric and eccentric diameters of the porous layers were raised. Another result we obtained is that the effects of the Reynolds number on increasing the average Nusselt number of the eccentric porous layer was higher than the concentric porous layer. Also, the effect of reducing the diameter on the increase of the Nusselt number in the constant Reynolds number is greater in the eccentric porous layer state in comparison to the concentric porous layer state [26].

Figs. 16 and 17 show the variation of the Nusselt numbers and the distribution of heat flux on the solid cylinder surface relative to the various eccentric porous layer diameters that were changing during the simulation. This was the main obtained result .

The average Nusselt number and the distribution of the heat flux have grown with increasing the center of the eccentric porous layer from the center of the solid cylinder. It also shows that whenever the eccentric porous layer was developed, the force convection heat transfer rate into the fluid zone increased. Previous works [23-25] have obtained the average Nusselt number distribution in the concentric porous layer, in this work we obtained the average Nusselt number distribution in the eccentric porous layer, which increased the Nusselt number in similar diameters compared to previous works. Also, the average Nusselt number and the distribution of the heat flux have grown with increasing the center of the eccentric porous layer from the center of the solid cylinder (Figs. 16 and 17).

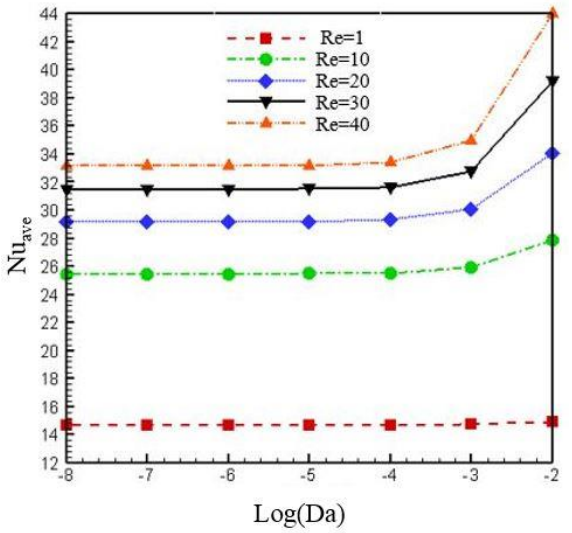

Fig. 14. The distribution of the average Nusselt number on the cylinder surface to different Darcy numbers.

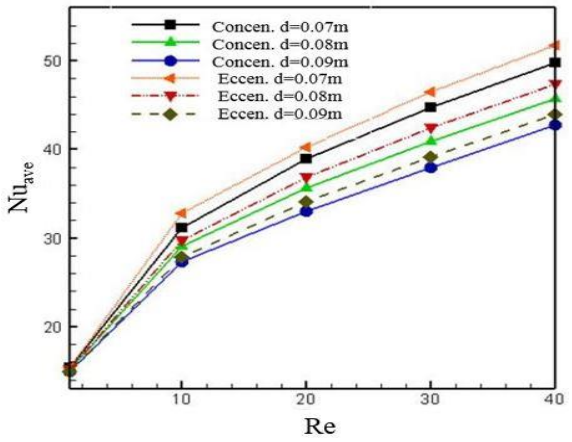

Fig. 15. The distribution of the average Nusselt number on the solid cylinder surface is different from the Reynolds numbers.

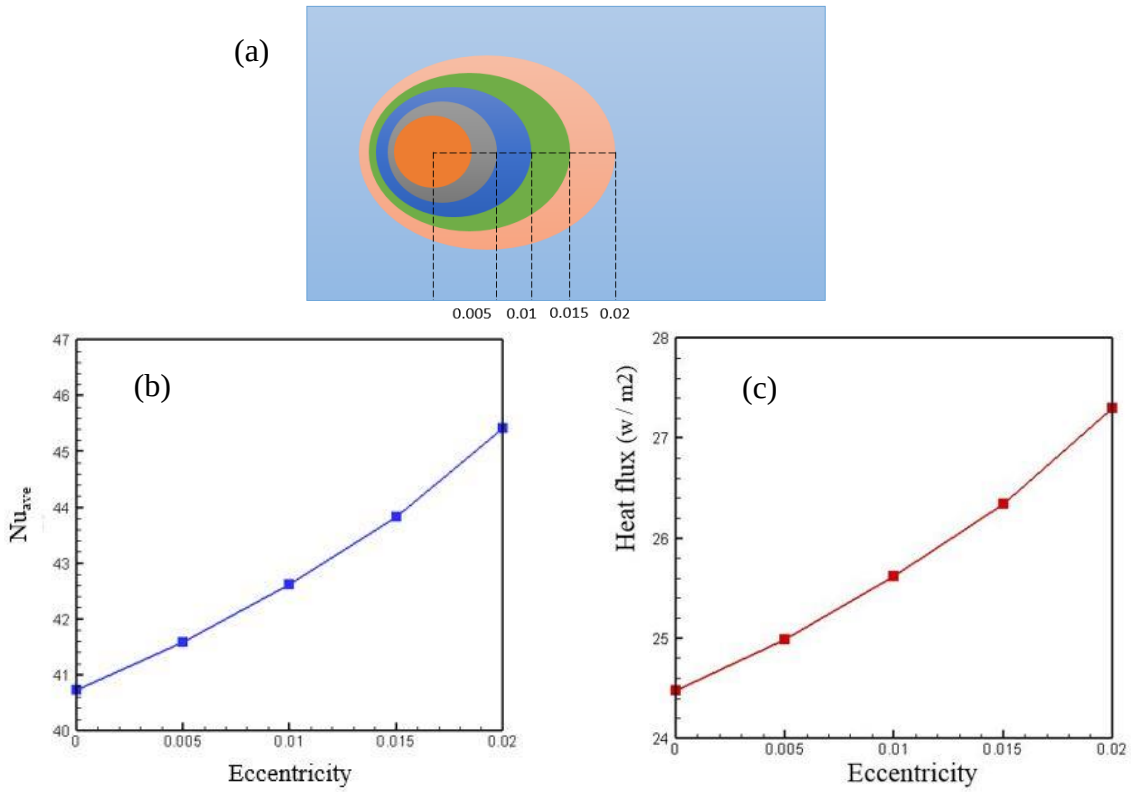

Fig. 16. (a) Schematic of solid cylinder surface relative to the various eccentric porous layer diameters, (b) Distribution of average Nusselt number on the cylinder surface with the various diameter of the eccentric porous layer, and (c) Distribution of heat flux on the cylinder surface with the various diameter of the eccentric porous layer.

4. Conclusions

In this study, the numerical simulations of heat transfer and fluid flow around the two-dimensional (2-D) cylinder wrapped around concentric and eccentric porous layers were conducted. The effects of different porous layer thickness, Darcy number, Reynolds number, permeability, and temperature and velocity (radial, tangential) distribution within the porous layer on the heat transfer and hydrodynamic flow were analyzed. In the first step of the study, we can find that the extent of the penetration of the fluid into the porous layer was increased with increasing the Darcy number. Also, the vortex formation length was developed by increasing the Reynolds number and decreasing the Darcy number. Then, it could be concluded that by increasing the Darcy number at a constant Reynolds number and a constant diameter of the porous layer, the heat flux rate passing through the surface of the constant temperature of the solid cylinder was raised. In the next stage of the numerical investigation, the results obviously demonstrate that in constant Reynolds numbers with the increase of Darcy number, the heat flux rate through the eccentric porous layer is more than the concentric porous layer. After that it could also be observed that with increasing the Darcy number (Log (Da) $\geq 10^{-4}$) and Reynolds number for all different values of diameters of concentric and eccentric porous layers around the solid cylinder, the average Nusselt number was raised. Ultimately, the findings of the study show that the average Nusselt number and the distribution of the heat flux have grown with increasing the center of the eccentric porous layer from the center of the solid cylinder.

Acknowledgements

The authors thank the chief of computer center of Department of Chemical Engineering, Shahid Bahonar University of Kerman, Kerman, Iran for supporting this work.

References

[1] S. Bhattacharyya, S. Dhinakaran and A. Khalili, "Fluid motion around and through a porous cylinder," *Chem. Eng. Sci*, Vol. 61, No. 13, pp. 44514461,(2006).

[2] S. Bhattacharyya and A. K. Singh, "Augmentation of heat transfer from a solid cylinder wrapped with a porous layer," *Int. J. Heat Mass Transfer*, Vol. 52, No. 7-8, pp.19912001, (2009).

[3] S. Rashidi, A. Tamayol, M. S. Valipour and N. Shokri, "Fluid flow and forced convection heat transfer around a solid cylinder wrapped with a porous ring," *Int. J. Heat Mass Transfer*, Vol. 63, No. 5, pp. 91100,(2013).

[4] A. Alinezhad, M. Khatibi and S. N. Ashrafizadeh, "Impact of asymmetry soft layers and ion partitioning on ionic current rectification in bipolar nanochannels," *J. Mol. Liq*, Vol. 347, No. 3, pp. 118324, (2022).

[5] A. Alinezhad and A. Alinezhad, "Influence of location junction on ion transfer behavior in conical nanopores with bipolar polyelectrolyte brushes," *Electrochimica. Acta*, Vol. 425, No. 2, pp.140699, (2022).

[6] A. Alinezhad, M. Khatibi and S. N. Ashrafizadeh," Ionic transfer behavior of bipolar nanochannels resembling PNP nanotransistor," *Electrochimica. Acta*, Vol. 460, No. 2, pp. 142625,(2023).

[7] D. K. Baghel, S. L. Sinha and S. K. Dewangan, "SST K-ω based air flow and heat transfer assessment in an infant incubator," *J. Comput. Appl. Res. Mech. Eng.*, Vol. 12, No. 2, pp. 161-175, (2023).

[8] S. M. M. Madani, J. Alinejad, Y. Rostamiyan and K. Fallah, "Lattice Boltzmann simulation inside a cavity: The effect of pipe profile on natural convection," *J. comput. Appl. Res. Mech. Eng.*, Vol. 13, No. 1, pp. 67-74, (2023).

[9] M. Sadegh Valipour and A. Zare Ghadi, "Numerical investigation of forced convective heat transfer around and through a porous circular cylinder with internal heat generation," *J. Heat Transfer*, Vol. 134, No. 6, (2012).

[10] F. M. Rong, Z. L. Guo, J. H. Lu and B. C. Shi, "Numerical simulation of the flow around a porous covering square cylinder in a channel via lattice Boltzmann method," *Int. J. Numer. Methods Fluids*, Vol. 65, No. 10, pp. 1217-1230, (2011).

[11] N. Alvandifar, M. Saffar-Avval and E. Amani, "Partially metal foam wrapped tube bundle as a novel generation of air cooled heat exchangers," *Int. J. Heat Mass Transfer*, Vol. 118, No. 2, pp. 171-181, (2018).

[12] M. Odabaee, K. Hooman and H. Gurgenci, "Metal foam heat exchangers for heat transfer augmentation from a cylinder in cross-flow," *Transp. Porous Media*, Vol. 86, No. 3, pp. 911-923, (2011).

[13] N. Rahmati, Z. Mansoori, M. Saffar-Avval and G. Ahmadi, "Numerical Study of Heat Transfer in Turbulent Cross-Flow Over Porous-Coated Cylinder." *J. Fluids Eng.*, Vol. 58042, No. 4, p. V01AT04A014, (2017).

[14] M. A. Saada, S. Chikh and A. Campo, "Natural convection around a horizontal solid cylinder wrapped with a layer of fibrous or porous material," *Int. J. Heat Fluid Flow*, Vol. 28, No. 3, pp. 483-495, (2007).

[15] G. F. Al-Sumaily, A. Nakayama, J. Sheridan and M. C. Thompson, "The effect of porous media particle size on forced convection from a circular cylinder without assuming local thermal equilibrium between phases," *Int. J. Heat Mass Transfer*, Vol. 55, No. 13-14, pp. 3366-3378,(2012).

[16] M. H. J. Pedras and M. J. S. de Lemos, "Macroscopic turbulence modeling for incompressible flow through undeformable porous media," *Int. J. Heat Mass Transfer*, Vol. 44, No. 6, pp. 1081-1093, (2001).

[17] K. Chen, L. Guo, X. Xie and W. Liu, "Experimental investigation on enhanced thermal performance of staggered tube bundles wrapped with metallic foam," *Int. J. Heat Mass Transfer*, Vol. 122, No. 3, pp. 459468,(2018).

[18] K. Al-Salem, H. F. Oztop and S. Kiwan, "Effects of porosity and thickness of porous sheets on heat transfer enhancement in a cross flow over heated cylinder," *I Int. Commun. Heat Mass Transfer*, Vol. 38, No. 9, pp. 1279-1282, (2011).

[19] V. V. Calmidi and R. L. Mahajan, "Forced convection in high porosity metal foams," *J. Heat Transfer*, Vol. 122, No. 3, pp. 557-565, (2000).

[20] C. Y. Zhao, T. Kim, T. J. Lu, and H. P. Hodson, "Thermal transport in high porosity cellular metal foams," *J. Thermophys. Heat Transfer*, Vol. 18, No. 3, pp. 309-317, (2004).

[21] E. Ebrahimi, Y. Amini, and G. Imani, "Heat transfer characteristics of a circular cylinder covered by a porous layer undergoing vortex-induced vibration," *Int. J. Therm.*, Vol. 166, No. 2, p. 106974, (2021).

[22] M. Mehdi Keshtkar and M. Dadkhodazadeh, "Thermal simulation of the symmetric and asymmetric arrangement of barriers on heat transfer enhancement in a porous gas heat exchanger," *J. Therm. Sci. Eng. Appl.*, Vol.10, No. 5, p. 051001, (2018).

[23] Y. Kaptan, E. Buyruk and A. Ecder, "Numerical investigation of fouling on cross-flow heat exchanger tubes with conjugated heat transfer approach," *Int. Commun. Heat Mass Transfer*, Vol. 35, No. 9, p. 11531158, (2008).

[24] Y. J. Zhuang, H. Z. Yu and Q. Y. Zhu, "Experimental and numerical investigations on the flow around and through the fractal soft rocks with water vapor absorption," *Int. J. Heat Mass Transfer*, Vol. 96, No. 3, pp. 413-429, (2016).

[25] H. Kaydani and A. Mohebbi, "Experimental and numerical study of the onset of transient natural convection in a fractured porous medium," *Transp. Porous Media*, Vol. 116, No. 2, pp. 923-939, (2017).

[26] X. Liu, D. Toghraie, M. Hekmatifar, O. A. Akbari, A. Karimipour and M. Afrand, "Numerical Investigation of Nanofluid Laminar Forced Convection Heat Transfer between Two Horizontal Concentric Cylinders in the Presence of Porous Medium," *J. Therm. Anal. Calorim*, Vol. 141, No. 3, pp. 2095-2108, (2020).

How to cite this paper:

Alireza Alinezhad, Ataallah Soltani Goharrizi and Ataallah Kamyabi, "Effect of concentric and eccentric porous layers on forced convection heat transfer and fluid flow around a solid cylinder,", *J. Comput. Appl. Res. Mech. Eng.*, Vol. 13, No. 2, pp. 191-206, (2024).

DOI: 10.22061/JCARME.2024.8784.2182

URL: https://jcarme.sru.ac.ir/?_action=showPDF&article=2055